

Airglow data-driven modeling over a period of three solar cycles

Š. Mackovjak^{1,3}, M. Varga², S. Hrivňak³, O. Palkoci³, G. G. Didebulidze⁴

¹Department of Space Physics, Institute of Experimental Physics, Slovak Academy of Sciences, Košice, Slovakia

²Department of Cybernetics and Artificial Intelligence, Faculty of Electrical Engineering and Informatics, Technical University of Košice, Košice, Slovakia

³GlobalLogic Slovakia s.r.o., Košice, Slovakia

⁴Georgian National Astrophysical Observatory, Ilia State University, Tbilisi, Georgia

Key Points:

- A data-driven model is able to represent complex physical phenomena
- Advanced machine learning techniques are effective for the development of the data-driven model
- Developed data-driven model visualizes airglow hourly intensities over a 30-year period

Corresponding author: Šimon Mackovjak, Institute of Experimental Physics SAS, Watsonova 47, 04001 Košice, Slovakia, mackovjak@saske.sk

16 **Abstract**

17 The Earth's upper atmosphere is a dynamic environment that is continuously affected
 18 by space weather from above and atmospheric processes from below. An effective way
 19 to observe this interface region is the monitoring of airglow. Since the 1950s, airglow emis-
 20 sions have been systematically measured by ground-based photometers in specific wave-
 21 length bands during the nighttime. The availability of the calibrated data from over 30
 22 years of photometric airglow measurements from Georgia, at wavelengths of 557.7 nm
 23 and 630.0 nm, enable us to investigate if a data-driven model based on advanced machine
 24 learning techniques can be successfully employed for modeling airglow intensities. A re-
 25 gression task was performed using the time series of space weather indices and thermosphere-
 26 ionosphere parameters. We have found that the developed data-driven model has good
 27 consistency with the commonly used airglow model and also captures airglow variations
 28 caused by cycles of solar activity and changes of the seasons. This enables us to visu-
 29 alize the green and red airglow variations over a period of three solar cycles with a one-
 30 hour time resolution.

31 **1 Introduction**

32 The Earth's upper atmosphere acts as an interface between processes in space and
 33 on Earth. It is a very dynamic environment continuously influenced by solar radiation
 34 and space weather from above and by atmospheric weather and electrical discharges from
 35 below (Pfaff, 2012). An effective way to monitor these dynamics during night-time pe-
 36 riods in the altitude range of 80–300 km is observation of airglow (Khomich et al., 2008).
 37 Airglow is a non-thermal emission of light originating from excited atomic or molecu-
 38 lar states. The source of the excitation, directly or indirectly, is the solar electromag-
 39 netic radiation (Savigny, 2017). The particular process responsible for the emission of
 40 airglow and the amount of this emission is mainly dependent on the composition and con-
 41 centrations of neutral constituents and ion/electron densities in the thermosphere-ionosphere
 42 system.

43 The longest detected airglow variation is connected to the 11-year long solar cy-
 44 cle. The correlation between the well-known atomic oxygen $\text{OI}(^1\text{D}_2 - ^1\text{S}_0)$ airglow emis-
 45 sion of the green line (557.7 nm) with sunspot area was revealed in 1935 (Rayleigh & Jones,
 46 1935). The connection of solar activity, expressed by solar flux index F10.7 was confirmed
 47 by extensive studies (Deutsch & Hernandez, 2003; Liu & Shepherd, 2008; Reid et al., 2014).

48 The authors provide clear evidence that the green line intensity is maximal during the
49 maximum of the solar cycle. The variations within the year (annual oscillation and semi-
50 annual oscillation) are associated with the yearly tilt and rotation of the Earth around
51 the Sun and also with the dynamics in the whole atmosphere, mainly driven by atmo-
52 spheric tides. The amplitude and maximum of a period are different for different loca-
53 tions. Shepherd et al. (2006) and Liu et al. (2008) used UARS/WINDII (Shepherd et
54 al., 1993) space-based observations of the green line in the years 1991–1997 to present
55 airglow variations during the year for different latitudes. The authors concluded that for
56 the equatorial region, semi-annual variation has maxima at equinoxes and for the mid-
57 latitude regions, the annual variation is dominant and has a maximum in autumn in the
58 northern hemisphere and in spring in the southern hemisphere. There are also shorter
59 and non-periodic variations in the upper atmosphere. The influence of geomagnetic storms
60 has been observed in airglow intensity measurements since the mid-twentieth century
61 (Silverman, 1970). During a geomagnetic storm, the density distribution of the ions and
62 neutral constituents in the upper atmosphere varies dramatically. Such variations may
63 have signatures in airglow emissions (Leonovich et al., 2011; Makela et al., 2014; Bag et
64 al., 2017).

65 Although some patterns in airglow variations were recognized, a clear physical ex-
66 planation is still missing. This is the consequence of the very high complexity of the en-
67 vironment and the fact that the response of airglow production might be not uniformly
68 related to a single process. Indeed, airglow intensity represents the continuous variation
69 of solar activity, solar wind, interplanetary magnetic field, magnetospheric drivers as well
70 as non-constant density and temperature conditions in the upper atmosphere together
71 with permanent vertical motions from lower atmosphere including tides, planetary waves,
72 and atmospheric gravity waves. The ionosphere-thermosphere system is also affected by
73 alteration of the global ionosphere electric potential and by various ionospheric insta-
74 bilities such as plasma bubbles and ionospheric scintillation (Eastes et al., 2019). As the
75 understanding of consequences of these processes is still not sufficient, the whole sub-
76 ject is very topical and it is an objective of several ground-based and space-based mis-
77 sions (e.g. Eastes et al., 2017; Immel et al., 2018; Hannawald et al., 2019; Mackovjak et
78 al., 2019; Wüst et al., 2019, and others).

79 Data-driven machine learning techniques have become effective tools in space sci-
80 ence in recent years (e.g., Ball & Brunner, 2010; George & Huerta, 2018; Zucker & Giryes,

2018, and others). It is mainly due to the fact that the huge amount of space data can be effectively processed by power-full computing units utilizing open source frameworks supported by technology giants (e.g. Pedregosa et al., 2011; Abadi et al., 2015; Paszke et al., 2017, and others). A comprehensive overview of the machine learning techniques and their application for space weather research is presented by Camporeale et al. (2018). The aim of this paper is to investigate if a data-driven approach using machine learning techniques can provide sufficient results of long-term airglow intensity modeling. The usefulness of this approach will be evaluated by its capability to reproduce generally known airglow variations as well as by comparison with the output from the Global Airglow (GLOW) model (Solomon et al., 1988; Solomon, 2017; Hirsch & Solomon, 2019). The data and machine learning methods used are described in Section 2. The obtained results and discussion are presented together in Section 3. Section 4 summarizes our work and describes the next steps in our research.

2 Data and Methods

Depending on the solar elevation, airglow can be categorized as dayglow, twilight-glow and nightglow (Savigny, 2017). Dayglow emission is the brightest but its observation is not straightforward due to the presence of direct and scattered light from the Sun. Therefore, every time the term airglow is used in this work, the nightglow (solar zenith angle (S_{ZA}) is higher than 108°) is considered. Our main focus is on atomic oxygen emissions - green line and red line with the wavelengths 557.7 nm and 630.0 nm, respectively. The details of their emission production mechanisms are presented in Khomich et al. (2008).

The main dataset used consists of calibrated photometric data of the airglow green line (557.7 nm) and airglow red line (630.0 nm) measured at Abastumani in Georgia (41.75° N, 42.82° E, 1,580 m a.s.l.) in the years 1957–1993 (Fishkova, 1983; Gudadze et al., 2007; Didebulidze et al., 2011; NDMC, (last access: November 30, 2020)). The measured intensities are in units of Rayleighs ($1 \text{ R} = 10^{10} \text{ photon m}^{-2} \text{ s}^{-1}$). They were acquired during the moonless (moon zenith angle (M_{ZA}) is higher than 90°) and cloudless conditions. The time resolution of the data is 6–15 minutes. For the purposes of this work, hourly averages were used within the time interval 1964–1993. The boxplots of the measured data are displayed in Figure 1. They represent the distributions of the measurements over the years. The total amount of data used is $\sim 3,850$ measurements, representing $\sim 8\%$ of all possible dark night hours (hours when $S_{ZA} > 108^\circ$ & $M_{ZA} > 90^\circ$) over a 30-year

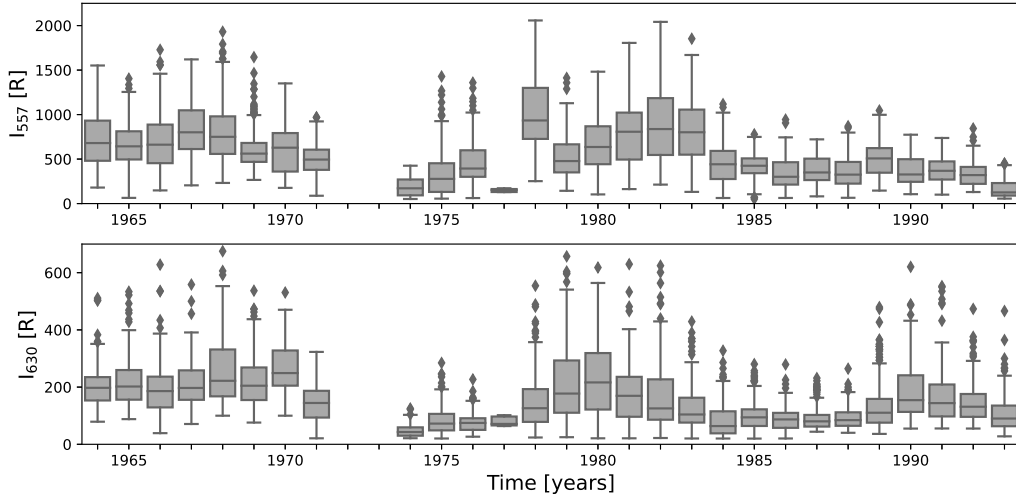


Figure 1. The box plots of the airglow measurements at Abastumani (Georgia) over the years 1964–1993. Only the hourly averages are considered where the sunless, moonless, and cloudless conditions are satisfied. Each interquartile range is represented by the particular box and the median of the distribution is marked with a horizontal dash. Distributions of the green line and red line intensities are displayed on the top and bottom, respectively.

113 period for this location. One of the goals of this work is to model the airglow green and
 114 red line intensities for the rest of the dark night hours (i.e. $\sim 92\%$) in this period.

115 In the data-driven modeling approach, the measured airglow intensities were used
 116 as labels. The features for the model were chosen from four categories: space weather
 117 indices, thermosphere parameters, ionosphere parameters, and Sun-Earth distance. These
 118 four categories cover the basic processes that affect airglow intensities. Although the ex-
 119 act physical relations between these features and labels are not considered here, these
 120 relations should be underlyingly present in the data. Machine learning techniques should
 121 be able to recognize these underlying relations and also model airglow intensities for pre-
 122 viously unseen feature values. For the appropriate feature selection, all available data
 123 from the OMNIWeb space weather database (King & Papitashvili, 2005), NRLMSISE-
 124 00 thermosphere model (Picone et al., 2002), and IRI-2016 ionosphere model (Bilitza et
 125 al., 2017) were explored. These data are accessible in hourly resolution. The availabil-
 126 ity of the features for a 30-year interval was considered in the feature selection process.
 127 The parameters of the neutral atmospheres and ionosphere are obtained for the altitudes
 128 95 km and 250 km for modeling green and red line, respectively. These are the altitudes

Table 1. The selected features for machine learning techniques to model airglow intensities

Feature	Units	Description	Source
F10.7 index	SFU	Solar radio flux per frequency ($\lambda = 10.7$ cm)	OMNIWeb ^a
Kp index		Geomagnetic planetary K-index	
Dst index	nT	Geomagnetic equatorial index	
Neutral Temperature	K	Temperature of neutral atmosphere	NRLMSISE-00 ^b
Total Mass Density	g/cm ³	Total mass density of neutral atmosphere	
O	N/cm ³	Atomic oxygen density	
O ₂	N/cm ³	Molecular oxygen density	
N	N/cm ³	Atomic nitrogen density	
N ₂	N/cm ³	Molecular nitrogen density	
H	N/cm ³	Atomic hydrogen density	
T _e	K	Temperature of electrons	IRI-2016 ^c
n _e	N/m ³	Density of electrons	
h _m F ₂	km	F ₂ layer peak height	
N _m F ₂	N/m ³	F ₂ layer peak density	
Sun-Earth	AU	Sun-Earth distance	PyEphem ^d

^aAvailable at: <https://omniweb.gsfc.nasa.gov/form/dx1.html> (King & Papitashvili, 2005)^bAvailable at: <https://ccmc.gsfc.nasa.gov/modelweb/models/nrlmsise00.php> (Picone et al., 2002)^cAvailable at: https://ccmc.gsfc.nasa.gov/modelweb/models/iri2016_vitmo.php (Bilitza et al., 2017)^dAvailable at: <https://pypi.org/project/pyephem>

129 of particular peak airglow layer emissions (Savigny, 2017). The feature selection was mainly
 130 induced by a current physical understanding of the features' influence on airglow pro-
 131 duction and also on automatic data characterization methods. The automatic methods
 132 as univariate feature selection and recursive selection of the features based on the model
 133 training process (Pedregosa et al., 2011) have been examined for the exclusion of the re-
 134 dundant features by quantification of their mutual correlation and by other statistical
 135 tests. The list of 15 features selected for our work is presented in Table 1. We would like
 136 to mention that no of the investigated feature had a significant correlation with airglow
 137 intensities. The absolute value of pairwise Pearson correlation coefficient is not higher
 138 than 0.26 for any pair of feature and label. It is noted that consideration of additional
 139 features did not lead to better results. This does not mean the irrelevancy of other in-
 140 dices such as e.g. the interplanetary magnetic field or solar wind parameters. These in-
 141 dices were excluded as their availability is less than 60% of the studied time interval.

142 The modeling of airglow intensities using the space weather indices, thermosphere-
 143 ionosphere parameters, and Sun-Earth distances as the input is indeed a regression prob-
 144 lem. Using known input and output values we would like to approximate the mapping
 145 function that could provide, with sufficient precision, the airglow intensities as the out-
 146 put for the previously unseen inputs. In the current work, we have employed the follow-
 147 ing supervised machine learning techniques for the regression problem: linear regression,
 148 Neural Networks, and the ensemble algorithms - Random Forest and XGboost. Ordi-
 149 nary least squares linear regression, as the common statistical approach in astronomy
 150 (Isobe et al., 1990), was used as the simplest technique. The Neural Network is one of
 151 the most popular machine learning techniques, although its use is still not typical for prob-
 152 lems where the features come from different distributions. It is based on the fact that
 153 every continuous real function over a compact set of real numbers can be approximated
 154 arbitrarily well by a function defined as a Neural Network with a high enough numbers
 155 of neurons. For more details refer to Cybenko (1989). In this work, we used a single hid-
 156 den layer feed-forward Neural Network with a number of neurons 128-128-1, hyperbolic
 157 tangent activation function, 300 learning epochs, and learning rate from 0.1 to 0.05 dur-
 158 ing the training. The choice of these hyperparameters was based on pure experimenta-
 159 tion with different values and optimizing for the metrics described below. The Random
 160 Forest technique (Tin Kam Ho, 1998; Breiman, 2001) is a combination of decision tree
 161 predictors. Indeed, it is an approach to average numerous decision trees to obtain min-

162 imal variance. In this work, we used the Random Forest regressor with 100 decision trees
 163 and 15 maximum tree depth. The Random Forest technique is not as sensitive to the
 164 specified hyper-parameters as Neural Network approach. Another very effective technique
 165 based on decision trees is Extreme Gradient Boosting - XGBoost (Chen & Guestrin, 2016).
 166 It is an ensemble method that is developed to prevent overfitting, handle missing val-
 167 ues, allow parallel processing, and perform cross-validation at each iteration. It tries to
 168 find an optimal output using the gradient descent algorithm to minimize the loss for the
 169 newly created model. In this work, we used XGBoost regression with squared loss, 0.05
 170 learning rate, and 15 maximum tree depth. All the methods mentioned above are im-
 171 plemented and available in the libraries of the Python programming language (Van Rossum
 172 & Drake, 2009) i.e. scikit-learn (Pedregosa et al., 2011) and Keras (Chollet, 2015). Here,
 173 we have provided only a brief description. The specific set-up of the machine learning
 174 techniques used and their hyper-parameters can be found in the Jupyter notebook that
 175 is available as online material to this article (SPACE::LAB, 2020).

176 In order to characterize the performance of the techniques used, the following met-
 177 rics were considered. The mean absolute error (MAE) represents the difference between
 178 the true label value y_i of the airglow intensity and the corresponding modeled value \hat{y}_i
 179 of the i -th sample. It is defined as:

$$180 \quad MAE(y, \hat{y}) = \frac{1}{n} \sum_{i=1}^n |y_i - \hat{y}_i|, \quad (1)$$

181 for n number of samples. Due to the reason that the absolute intensities of green and
 182 red airglow lines are different, we introduced also a relative metric the mean absolute
 183 percentage error (MAPE). It allows us to compare the performance of the techniques used
 184 for both airglow lines. By assumption that the measured airglow intensity y_i will be al-
 185 ways higher than zero, the MAPE is defined as:

$$186 \quad MAPE(y, \hat{y}) = \frac{100\%}{n} \sum_{i=1}^n \frac{|y_i - \hat{y}_i|}{y_i}. \quad (2)$$

187 Due to the complexity of the upper atmosphere environment, the commonly used
 188 models applied for calculation of airglow intensities are limited and do not contain all
 189 the relevant processes. One of the most used, the Global Airglow (GLOW) model (Solomon
 190 et al., 1988; Solomon, 2017; Hirsch & Solomon, 2019) provides emission rates for most
 191 prominent airglow lines for particular altitude, latitude, longitude, and time. It uses en-
 192 ergetic inputs from the Sun and aurora and also thermospheric parameters. It can also

193 employ the output from general atmosphere circulation models such as the Thermosphere-
 194 Ionosphere-Electrodynamics General Circulation Model (TIE-GCM) (Roble et al., 1988;
 195 Qian et al., 2014). The simulated airglow brightness over the whole Earth’s disk is qual-
 196 itatively consistent with measurements from the most recent airglow space mission GOLD
 197 (Global-scale Observations of the Limb and Disk) (Gan et al., 2020).

198 **3 Results and Discussion**

199 The objective of the presented work is to model the intensities of the airglow green
 200 line (557.7 nm) and red line (630.0 nm) for the period 1964–1993. For this purpose, we
 201 employed the data and techniques described in Section 2. It is noted that the main dataset
 202 was split into a subset for training and a subset for testing of each particular technique.
 203 The comparison of the performance of the machine learning techniques used against the
 204 subset for testing is presented in Table 2.

Table 2. The performance of machine learning techniques used for modeling of green (557.7 nm) and red (630.0 nm) airglow lines intensities.

	I 557		I 630	
	MAE	MAPE	MAE	MAPE
Baseline	265 R	78 %	84 R	86 %
Lin. Regression	247 R	65 %	77 R	72 %
Neural Network	146 R	95 %	63 R	90 %
Random Forest	102 R	23 %	53 R	41 %
XGBoost	88 R	16 %	48 R	32 %

205 For the purposes of quantifying the methods’ performance, the results from base-
 206 line model are also listed. They were obtained by considering simple average of the val-
 207 ues of training labels as the modeled value \hat{y}_i . As expected, the lowest performance was
 208 obtained for the simplest method - linear regression. The Neural Network model pro-
 209 vides significantly better results for MAE but even worse results for MAPE than the base-
 210 line. This is the consequence of the fact that for some low values of y_i the modeled value
 211 of \hat{y}_i might be relatively much more different although in absolute values this difference
 212 is not so high. It is a good example that both MAE and MAPE metrics should be pre-

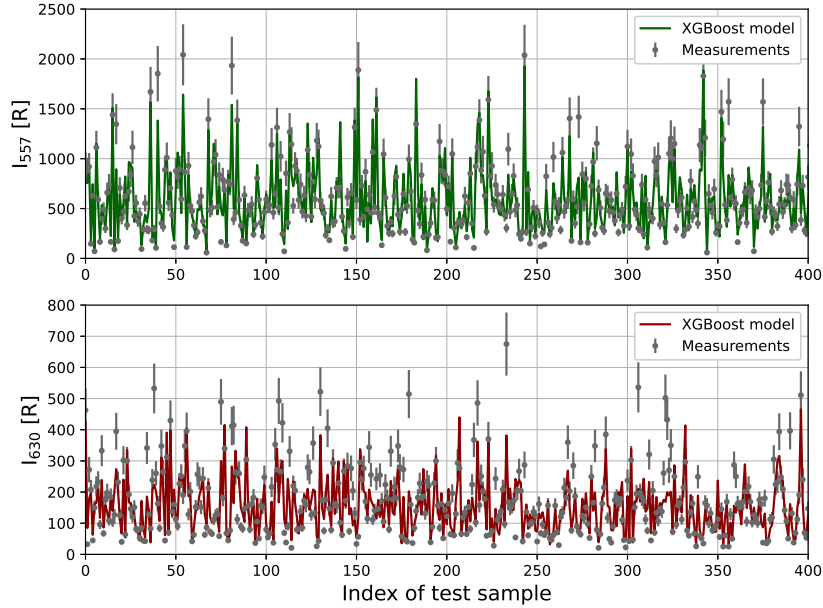


Figure 2. The performance of XGBoost model on the testing subset for green (top) and red (bottom) airglow lines intensities. The samples for the testing subset were selected randomly from all the available data. Only half of the testing subset is displayed to provide better visualization. The accuracy of the model against measurements is expressed in Table 2.

213 sented together. The evidence that the neural networks might be outperformed by tech-
 214 niques based on decision trees for limited datasets is well known (Wang et al., 2018). This
 215 is also the case of our work where the Random Forest technique provides lower MAE and
 216 MAPE than the Neural Network. Furthermore, the Random Forest training process was
 217 roughly ~ 20 times computationally more efficient than the training process of the Neu-
 218 ral Network. As the XGBoost is even more advanced than Random Forest technique,
 219 it was expected that it will have even better performance. This assumption was confirmed
 220 and the best-performing technique in our work was the XGBoost. The MAPE for green
 221 and red airglow lines were 16% and 32%, respectively. The visualization of XGBoost per-
 222 formance on the testing subset is displayed in Figure 2. Considering the data measure-
 223 ment uncertainty level of 10–15% (Fishkova, 1983), the machine learning model performs
 224 sufficiently well to qualitatively express the airglow variations.

225 The results of the modeled intensities for green and red airglow lines over the whole
 226 studied period 1964–1993 is in Figure 3. The modeled values were obtained using all avail-
 227 able needed input features and by the prediction of the trained machine learning model

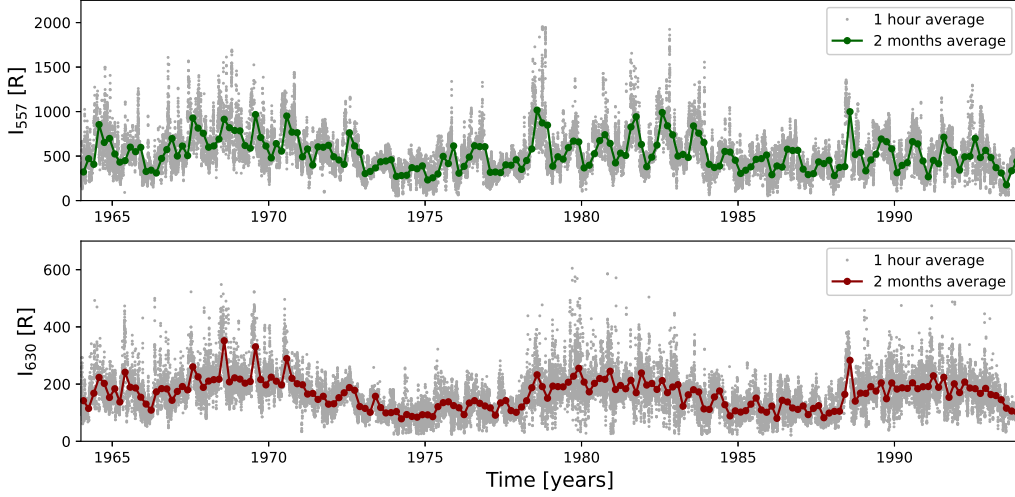


Figure 3. Visualization of airglow intensities modeled by the XGBoost technique for the location Abastumani (Georgia) over the years 1964–1993. The averages over 1 hour and 2 months for green (*top*) and red (*bottom*) airglow lines are displayed. Only dark night hours are considered.

228 which is based on the XGBoost technique. Figure 3 represents the achievement of one
 229 of this work’s goals as it contains averaged intensities of green and red airglow lines for
 230 46,223 hours i.e. for 100% of all dark night hours within 1964–1993 period. Figure 3 serves
 231 as the visualization of the green and red airglow lines intensities variations that are dis-
 232 played for a continuous period over three solar cycles. To our knowledge, airglow vari-
 233 ation visualization for a such long period and such time resolution has not been published
 234 thus far.

235 To examine the credibility of the results generated by our machine learning model,
 236 we have compared them with the results of the GLOW model. These results were ob-
 237 tained by the default setup of the GLOW model. The calculated volume emission rates
 238 were integrated over all altitudes to achieve values that might be compared with the mea-
 239 sured airglow data. For the same testing dataset as was used for Table 2, the GLOW
 240 model achieved as follows for the green line: MAE equals 280 R and MAPE equals 89%,
 241 for the red line: MAE equals 109 R and MAPE equals 84%. These values are not as good
 242 as the results of our machine learning model. This can be explained by the fact that the
 243 particular measured data might be influenced by phenomena that are not yet considered
 244 in the GLOW model. The performance of our machine learning model and the GLOW
 245 model is presented in Figure 4. This represents that both models are qualitatively in good

246 agreement. The correlation coefficients of simulated intensities for the GLOW model and
 247 our machine learning model based on XGBoost averaged over 2 months and consider-
 248 ing a linear least-squares regression are 0.48 and 0.54 for green and red line, respectively.
 249 It is an important result that the data-driven model can provide valuable results even
 250 with a comparison of the physical model generally used. Even-more, as displayed in Fig-
 251 ure 4, the data-driven model is less uniform than the physical model and might be more
 252 consistent with the real variability expressed by the measurements. To validate our data-
 253 driven model, we made an experiment where we split the main dataset for the subset for
 254 training and testing covering the years 1964–1973 (i.e. 33% of the previously used dataset)
 255 and for the subset for validation covering the years 1974–1993. The new model was trained
 256 and tested by using the training and testing subsets only. Its performance was then in-
 257 vestigated by the validation subset. The MAE and MAPE for the green airglow line were
 258 301 R and 111%, respectively. The MAE and MAPE for the red airglow line were 115 R
 259 and 152%, respectively. The mean errors are significantly higher than values in Table
 260 2 but this was expected because we used only data from a 10-year period for the train-
 261 ing and testing process. The metrics for the GLOW model by using the same validation
 262 dataset were very similar. The MAE and MAPE for the green airglow line were 308 R
 263 and 117%, respectively. The MAE and MAPE for the red airglow line were 112 R and
 264 104%, respectively. This demonstrates that for a completely unseen time period our data-
 265 driven approach is still able to produce comparable results to the GLOW model. It is
 266 interesting that the correlation coefficients are now higher and are equal to 0.75 and 0.73
 267 for green and red line, respectively. This means that when we used less data for train-
 268 ing of our model its results are even more similar to the results of the GLOW model. It
 269 is consistent with our previous assumption that the GLOW model as well as our model
 270 trained on only a 10-year period do not consider all phenomena influenced airglow in-
 271 tensities. After all it is important to note, the GLOW model is much more general than
 272 the particular data-driven model and can be used for any location and time because it
 273 does not require any measured airglow data for the input.

274 Another examination of the credibility of our machine learning model is its abil-
 275 ity to express the airglow variations briefly presented in Section 1. The airglow modu-
 276 lation by an 11-year solar cycle is visible in Figure 3 at a glance. The green and red air-
 277 glow lines intensities are maximal for the periods around the maximums of solar activ-
 278 ity in the years 1969, 1980, and 1991, which is consistent with expectations. The annual

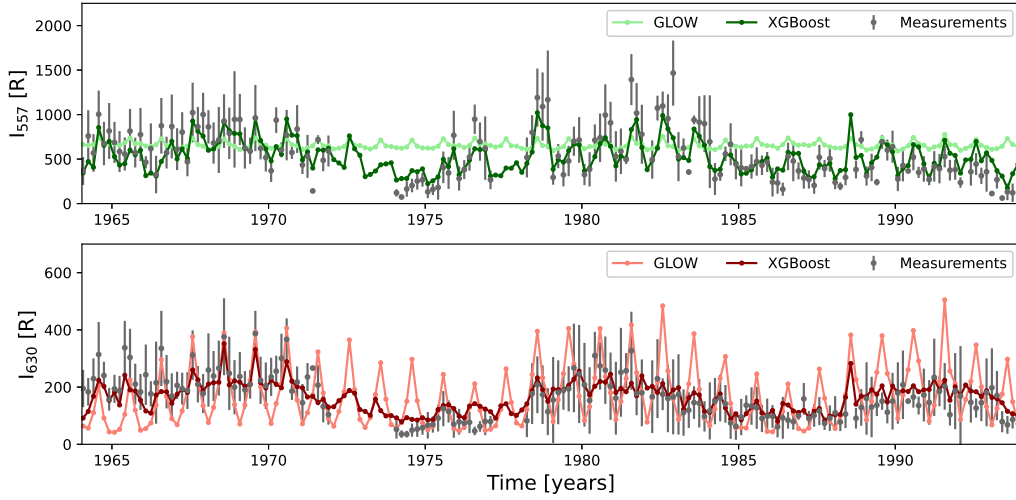


Figure 4. The time series of green (*top*) and red (*bottom*) airglow lines for the period 1964–1993. The 2-month averages of calculated intensities using the GLOW model and our data-driven model based on the XGBoost technique. The 2-month averages of measurements from Abastumani (Georgia) (see Figure 1) are displayed together with their standard deviations.

279 variation can be also recognized in Figure 3. According to previous studies (Shepherd
 280 et al., 2006) this variation of green line intensities should have its minimum in spring and
 281 maximum in autumn for the considered location in the middle latitudes of the north-
 282 ern hemisphere. The results of our data-driven model presented in Figure 5 (*top*) are
 283 consistent with these studies. The assumption for the red airglow line for the considered
 284 location is that the maximum average intensity should be in summer and the minimum
 285 near equinoxes (Khomich et al., 2008). The results presented in Figure 5 (*bottom*) are
 286 also consistent with this assumption. We note, there are much more airglow variations
 287 underlyingly present in Figures 3 and 5. They might be recognized by further investi-
 288 gation of the developed data-driven model results. These analyses and comparison with
 289 various measurements, as done by other authors (e.g. Deutsch & Hernandez, 2003; Gu-
 290 dadze et al., 2008, and others), are objectives for future publication.

291 4 Conclusions

292 Space data are of irreplaceable value as they provide information about phenom-
 293 ena that can not be repeated. However, the occurrence of missing measurements and gaps
 294 in the time series is very common. This is especially true for the ground-based measure-

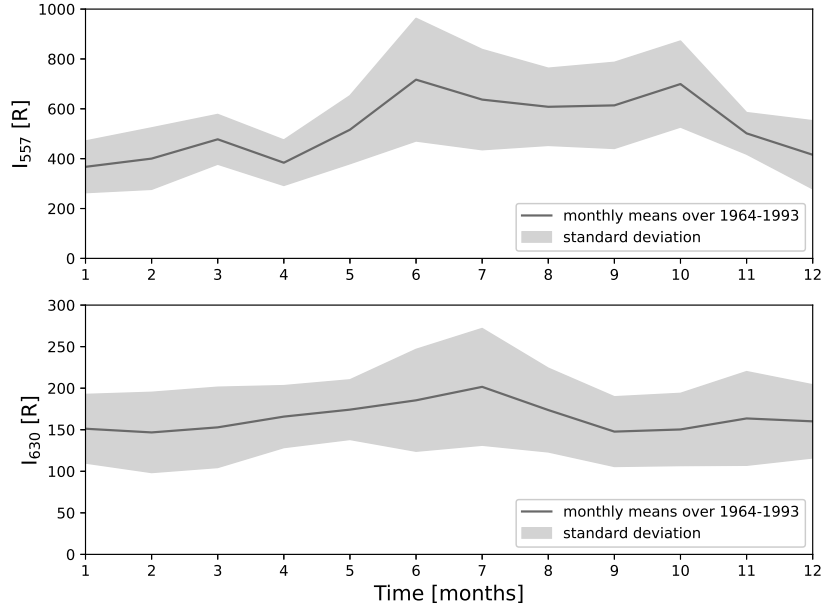


Figure 5. The average intensities calculated by a data-driven model based on the XGBoost technique for Abastumani (Georgia). The intensities were averaged over a particular month and for the years 1964–1993. The standard deviations from the mean values over the years are also displayed.

295 ments where the observations are limited by the weather conditions. We have used the
 296 most recent machine learning techniques to solve the regression problem and to model
 297 the missing intensities of green and red airglow lines for the location Abastumani (Geor-
 298 gia) over the time period 1964–1993. For this purpose, a data-driven approach was con-
 299 ducted. The photometric airglow measurements were used as the labels and space weather
 300 indices, thermosphere-ionosphere parameters, and Sun-Earth distances were used as the
 301 features. The techniques of Linear Regression, Neural Network, Random Forest, and XG-
 302 Boost were employed and their performance was compared against the testing dataset.
 303 The model based on the XGBoost technique outperformed the others and provided mean
 304 absolute percentage error (MAPE) 16% and 32% for green and airglow lines, respectively.
 305 This performance is sufficient to qualitatively express the overall airglow variation. This
 306 fact constitutes the ability of the modeled data to represent the missing measurements
 307 with the mentioned uncertainties. The obtained data visualize the variations in the in-
 308 tensities of the green and red airglow lines over the period of three solar cycles. The re-

309 sults from the data-driven model are consistent with the GLOW model (Solomon, 2017)
310 and depict the main variations related to solar activity and the seasons.

311 The modeled airglow data might contribute to understanding the processes in the
312 interface region between the space environment and Earth’s atmosphere. Even more, the
313 absolute values of airglow intensities and the range of their variation are crucial for fu-
314 ture missions like EUSO-SPB2 (Wiencke, 2019) and POEMMA (NASA Probe Study re-
315 port, 2020; Anchordoqui et al., 2020). These missions are designed to observe extensive
316 air showers induced by ultra-high energy cosmic rays and to observe Cherenkov light in-
317 duced by cosmic neutrinos. Indeed, airglow emissions set the energy threshold of the events
318 that could be recognized in the Earth’s night atmosphere by observation from orbit (JEM-
319 EUSO collaboration, 2019; Krizmanic, 2021). For this purpose we plan to extend the vi-
320 sualization of the airglow intensities for the years 1994–2020 as the input features should
321 be available. We would like to also focus on the short time periods when the airglow in-
322 tensities were significantly high and to investigate the possible explanations of these spe-
323 cific events.

324 **Acknowledgments**

325 These airglow studies are supported by the government of Slovakia through an ESA con-
326 tract under the PECS (Plan for European Cooperating States). ESA Disclaimer: The
327 view expressed herein can in no way be taken to reflect the official opinion of the Eu-
328 ropean Space Agency. The studies of Sun-Earth connection are supported by the VEGA
329 grant agency project 2/0155/18. The work is also supported by the Slovak Academy of
330 Sciences MVTs JEM-EUSO. The studies related to machine learning techniques are sup-
331 ported by GlobalLogic Slovakia s.r.o. Data Availability Statement: The airglow data were
332 provided by G. Didebulidze and are publicly available through the NDMC database (<https://ndmc.dlr.de>).
333 The data of space weather, thermosphere, and ionosphere parameters are publicly avail-
334 able through the NASA data centers (<https://omniweb.gsfc.nasa.gov>, <https://ccmc.gsfc.nasa.gov>).
335 The presented results can be reproduced by the Jupyter notebook publicly available at
336 <https://doi.org/10.5281/zenodo.4306913>.

337 **References**

338 Abadi, M., Agarwal, A., Barham, P., Brevdo, E., Chen, Z., Citro, C., . . . Zheng, X.
339 (2015). *TensorFlow: Large-scale machine learning on heterogeneous systems*.

- 340 (Software available from tensorflow.org)
- 341 Anchordoqui, L. A., Bergman, D. R., Bertaina, M. E., Fenu, F., Krizmanic,
 342 J. F., Liberatore, A., ... Wiencke, L. (2020, January). Performance
 343 and science reach of the Probe of Extreme Multimessenger Astrophysics
 344 for ultrahigh-energy particles. *Physical Review D*, *101*(2), 023012. doi:
 345 10.1103/PhysRevD.101.023012
- 346 Bag, T., Singh, V., & Krishna, M. S. (2017). Study of atomic oxygen greenline day-
 347 glow emission in thermosphere during geomagnetic storm conditions. *Advances*
 348 *in Space Research*, *59*(1), 302 - 310. doi: <https://doi.org/10.1016/j.asr.2016.08>
 349 .037
- 350 Ball, N. M., & Brunner, R. J. (2010, January). Data Mining and Machine Learning
 351 in Astronomy. *International Journal of Modern Physics D*, *19*(7), 1049-1106.
 352 doi: 10.1142/S0218271810017160
- 353 Bilitza, D., Altadill, D., Truhlik, V., Shubin, V., Galkin, I., Reinisch, B., & Huang,
 354 X. (2017). International reference ionosphere 2016: From ionospheric cli-
 355 mate to real-time weather predictions. *Space Weather*, *15*(2), 418-429. doi:
 356 <https://doi.org/10.1002/2016SW001593>
- 357 Breiman, L. (2001). Random forests. *Machine Learning*, *45*(1), 5-32. doi: 10.1023/
 358 A:1010933404324
- 359 Camporeale, E., Wing, S., & Johnson, J. (2018). *Machine learning techniques for*
 360 *space weather*. Elsevier. doi: <https://doi.org/10.1016/C2016-0-01976-9>
- 361 Chen, T., & Guestrin, C. (2016). XGBoost: A scalable tree boosting system. In
 362 *Proceedings of the 22nd acm sigkdd international conference on knowledge*
 363 *discovery and data mining* (pp. 785-794). New York, NY, USA: ACM. doi:
 364 10.1145/2939672.2939785
- 365 Chollet, F. e. a. (2015). *Keras*. <https://keras.io>.
- 366 Cybenko, G. (1989, December 1). Approximation by superpositions of a sigmoidal
 367 function. *Mathematics of Control, Signals, and Systems (MCSS)*, *2*(4), 303-
 368 314. doi: 10.1007/BF02551274
- 369 Deutsch, K. A., & Hernandez, G. (2003, December). Long-term behavior of the OI
 370 558 nm emission in the night sky and its aeronomical implications. *Journal of*
 371 *Geophysical Research (Space Physics)*, *108*, 1430. doi: 10.1029/2002JA009611
- 372 Didebulidze, G. G., Lomidze, L. N., Gudadze, N. B., Pataraya, A. D., & Todua, M.

- 373 (2011). Long-term changes in the nightly behaviour of the oxygen red 630.0
 374 nm line nightglow intensity and trends in the thermospheric meridional wind
 375 velocity. *International Journal of Remote Sensing*, *32*(11), 3093-3114. doi:
 376 10.1080/01431161.2010.541523
- 377 Eastes, R. W., McClintock, W. E., Burns, A. G., Anderson, D. N., Andersson, L.,
 378 Codrescu, M., ... Oberheide, J. (2017, October). The Global-Scale Observa-
 379 tions of the Limb and Disk (GOLD) Mission. *Space Sci. Rev.*, *212*, 383-408.
 380 doi: 10.1007/s11214-017-0392-2
- 381 Eastes, R. W., Solomon, S. C., Daniell, R. E., Anderson, D. N., Burns, A. G., Eng-
 382 land, S. L., ... McClintock, W. E. (2019). Global-scale observations of the
 383 equatorial ionization anomaly. *Geophysical Research Letters*, *46*(16), 9318-
 384 9326. doi: 10.1029/2019GL084199
- 385 Fishkova, L. M. (1983). *The night airglow of the earth mid-latitude upper atmo-*
 386 *sphere.*
- 387 Gan, Q., Eastes, R. W., Burns, A. G., Wang, W., Qian, L., Solomon, S. C., ... Mc-
 388 Clintock, W. E. (2020). First synoptic observations of geomagnetic storm
 389 effects on the global-scale oi 135.6-nm dayglow in the thermosphere by the
 390 gold mission. *Geophysical Research Letters*, *47*(3), e2019GL085400. doi:
 391 10.1029/2019GL085400
- 392 George, D., & Huerta, E. (2018). Deep learning for real-time gravitational wave
 393 detection and parameter estimation: Results with advanced ligo data. *Physics*
 394 *Letters B*, *778*, 64 - 70. doi: <https://doi.org/10.1016/j.physletb.2017.12.053>
- 395 Gudadze, N. B., Didebulidze, G. G., Javakhishvili, G. S., Shepherd, M. G., & Var-
 396 dosanidze, M. V. (2007, February). Long-term variations of the oxygen red 630
 397 nm line nightglow intensity. *Canadian Journal of Physics*, *85*(2), 189-198. doi:
 398 10.1139/P07-032
- 399 Gudadze, N. B., Didebulidze, G. G., Lomidze, L. N., Javakhishvili, G. S., Marsag-
 400 ishvili, M. A., & Todua, M. (2008). Different long-term trends of the
 401 oxygen red 630.0 nm line nightglow intensity as the result of lowering
 402 the ionosphere f2 layer. *Annales Geophysicae*, *26*(8), 2069-2080. doi:
 403 10.5194/angeo-26-2069-2008
- 404 Hannawald, P., Schmidt, C., Sedlak, R., Wüst, S., & Bittner, M. (2019). Seasonal
 405 and intra-diurnal variability of small-scale gravity waves in oh airglow at two

- 406 alpine stations. *Atmospheric Measurement Techniques*, 12(1), 457–469. doi:
407 10.5194/amt-12-457-2019
- 408 Hirsch, M., & Solomon, S. (2019, September). *space-physics/ncar-glow*. Zenodo. doi:
409 10.5281/zenodo.3463662
- 410 Immel, T. J., England, S. L., Mende, S. B., Heelis, R. A., Englert, C. R., Edel-
411 stein, J., ... Sirk, M. M. (2018, February). The Ionospheric Connection
412 Explorer Mission: Mission Goals and Design. *Space Sci. Rev.*, 214, 13. doi:
413 10.1007/s11214-017-0449-2
- 414 Isobe, T., Feigelson, E. D., Akritas, M. G., & Babu, G. J. (1990, November). Linear
415 Regression in Astronomy. I. *Astrophys. J.*, 364, 104. doi: 10.1086/169390
- 416 JEM-EUSO collaboration. (2019, September). Ultra-violet imaging of the
417 night-time earth by EUSO-Balloon towards space-based ultra-high en-
418 ergy cosmic ray observations. *Astroparticle Physics*, 111, 54-71. doi:
419 10.1016/j.astropartphys.2018.10.008
- 420 Khomich, V. Y., Semenov, A. I., & Shefov, N. N. (2008). *Airglow as an Indicator of*
421 *Upper Atmospheric Structure and Dynamics*. Springer-Verlag.
- 422 King, J. H., & Papitashvili, N. E. (2005). Solar wind spatial scales in and compar-
423 isons of hourly wind and ace plasma and magnetic field data. *Journal of Geo-*
424 *physical Research: Space Physics*, 110(A2). doi: 10.1029/2004JA010649
- 425 Krizmanic, J. F. (2021). Space-based extensive air shower optical cherenkov
426 and fluorescence measurements using sipm detectors in context of poemma.
427 *Nuclear Instruments and Methods in Physics Research Section A: Accelera-*
428 *tors, Spectrometers, Detectors and Associated Equipment*, 985, 164614. doi:
429 <https://doi.org/10.1016/j.nima.2020.164614>
- 430 Leonovich, L. A., Mikhalev, A. V., & Leonovich, V. A. (2011, Aug 17). The 557.7
431 and 630-nm atomic oxygen midlatitude airglow variations associated with
432 geomagnetic activity. *Atmospheric and Oceanic Optics*, 24(4), 396. doi:
433 10.1134/S1024856011040105
- 434 Liu, G., & Shepherd, G. G. (2008). An investigation of the solar cycle impact on the
435 lower thermosphere o(1s) nightglow emission as observed by windii/uars. *Ad-*
436 *vances in Space Research*, 42(5), 933 - 938. doi: [https://doi.org/10.1016/j.asr](https://doi.org/10.1016/j.asr.2007.10.008)
437 [.2007.10.008](https://doi.org/10.1016/j.asr.2007.10.008)
- 438 Liu, G., Shepherd, G. G., & Roble, R. G. (2008). Seasonal variations of the night-

- 439 time o(1s) and oh airglow emission rates at mid-to-high latitudes in the con-
 440 text of the large-scale circulation. *Journal of Geophysical Research: Space*
 441 *Physics*, 113(A6). doi: 10.1029/2007JA012854
- 442 Mackovjak, Š., Bobík, P., Baláž, J., Strhářský, I., Putiš, M., & Gorodetzky,
 443 P. (2019, April). Airglow monitoring by one-pixel detector. *Nuclear*
 444 *Instruments and Methods in Physics Research A*, 922, 150-156. doi:
 445 10.1016/j.nima.2018.12.073
- 446 Makela, J. J., Harding, B. J., Meriwether, J. W., Mesquita, R., Sanders, S., Ridley,
 447 A. J., ... Martinis, C. R. (2014). Storm time response of the midlatitude
 448 thermosphere: Observations from a network of fabry-perot interferometers.
 449 *Journal of Geophysical Research: Space Physics*, 119(8), 6758-6773. doi:
 450 10.1002/2014JA019832
- 451 NASA Probe Study report. (2020). *POEMMA: Probe of Extreme Multi-Messenger*
 452 *Astrophysics*. [https://smd-prod.s3.amazonaws.com/science-pink/
 453 s3fs-public/atoms/files/1_POEMMA_Study_Rpt_0.pdf](https://smd-prod.s3.amazonaws.com/science-pink/s3fs-public/atoms/files/1_POEMMA_Study_Rpt_0.pdf).
- 454 NDMC. ((last access: November 30, 2020)). *The Network for the Detection of Meso-*
 455 *spheric Change (NDMC)*, available at. <https://ndmc.dlr.de>.
- 456 Paszke, A., Gross, S., Chintala, S., Chanan, G., Yang, E., DeVito, Z., ... Lerer, A.
 457 (2017). *Automatic differentiation in pytorch*.
- 458 Pedregosa, F., Varoquaux, G., Gramfort, A., Michel, V., Thirion, B., Grisel, O., ...
 459 Duchesnay, E. (2011). Scikit-learn: Machine learning in Python. *Journal of*
 460 *Machine Learning Research*, 12, 2825–2830.
- 461 Pfaff, R. F. (2012, June). The Near-Earth Plasma Environment. *Space Sci. Rev.*,
 462 168, 23-112. doi: 10.1007/s11214-012-9872-6
- 463 Picone, J. M., Hedin, A. E., Drob, D. P., & Aikin, A. C. (2002). Nrlmsise-00 em-
 464 pirical model of the atmosphere: Statistical comparisons and scientific issues.
 465 *Journal of Geophysical Research: Space Physics*, 107(A12), SIA 15-1-SIA
 466 15-16. doi: 10.1029/2002JA009430
- 467 Qian, L., Burns, A. G., Emery, B. A., Foster, B., Lu, G., Maute, A., ... Wang,
 468 W. (2014). The ncar tie-gcm. In *Modeling the ionosphere-thermosphere*
 469 *system* (p. 73-83). American Geophysical Union (AGU). doi: 10.1002/
 470 9781118704417.ch7
- 471 Rayleigh, L., & Jones, H. S. (1935, Aug). The Light of the Night-Sky: Analysis of

- 472 the Intensity Variations at Three Stations. *Proceedings of the Royal Society of*
 473 *London Series A*, 151(872), 22-55. doi: 10.1098/rspa.1935.0133
- 474 Reid, I. M., Spargo, A. J., & Woithe, J. M. (2014). Seasonal variations of the
 475 nighttime O (1S) and OH (8-3) airglow intensity at Adelaide, Australia.
 476 *Journal of Geophysical Research: Atmospheres*, 119(11), 6991–7013. doi:
 477 10.1002/2013JD020906
- 478 Roble, R. G., Ridley, E. C., Richmond, A. D., & Dickinson, R. E. (1988). A coupled
 479 thermosphere/ionosphere general circulation model. *Geophysical Research Let-*
 480 *ters*, 15(12), 1325-1328. doi: 10.1029/GL015i012p01325
- 481 Savigny, C. v. (2017, Oct 17). Airglow in the earth atmosphere: basic characteris-
 482 tics and excitation mechanisms. *ChemTexts*, 3(4), 14. doi: 10.1007/s40828-017
 483 -0051-y
- 484 Shepherd, G., Thuillier, G., Gault, W., Solheim, B., Hersom, C., Alunni, J., ...
 485 Wimperis, J. (1993, 06). Windii, the wind imaging interferometer on the upper
 486 atmosphere research satellite. *J. Geophys. Res.*, 98. doi: 10.1029/93JD00227
- 487 Shepherd, G. G., Cho, Y.-M., Liu, G., Shepherd, M. G., & Roble, R. G. (2006,
 488 December). Airglow variability in the context of the global mesospheric circu-
 489 lation. *Journal of Atmospheric and Solar-Terrestrial Physics*, 68, 2000-2011.
 490 doi: 10.1016/j.jastp.2006.06.006
- 491 Silverman, S. M. (1970, October). Night Airglow Phenomenology. *Space Sci. Rev.*,
 492 11, 341-379. doi: 10.1007/BF00241526
- 493 Solomon, S. C. (2017). Global modeling of thermospheric airglow in the far ultravi-
 494 olet. *Journal of Geophysical Research: Space Physics*, 122(7), 7834-7848. doi:
 495 10.1002/2017JA024314
- 496 Solomon, S. C., Hays, P. B., & Abreu, V. J. (1988). The auroral 6300 Å emission:
 497 Observations and modeling. *Journal of Geophysical Research: Space Physics*,
 498 93(A9), 9867-9882. doi: 10.1029/JA093iA09p09867
- 499 SPACE::LAB. (2020, December). *space-lab-sk/airglow_data-driven_model: First re-*
 500 *lease*. Zenodo. Retrieved from <https://doi.org/10.5281/zenodo.4306913>
 501 doi: 10.5281/zenodo.4306913
- 502 Tin Kam Ho. (1998). The random subspace method for constructing decision
 503 forests. *IEEE Transactions on Pattern Analysis and Machine Intelligence*,
 504 20(8), 832-844.

- 505 Van Rossum, G., & Drake, F. L. (2009). *Python 3 reference manual*. Scotts Valley,
506 CA: CreateSpace.
- 507 Wang, S., Aggarwal, C., & Liu, H. (2018, 10). Random-forest inspired neural net-
508 works. *ACM Transactions on Intelligent Systems and Technology*, 9. doi: 10
509 .1145/3232230
- 510 Wiencke, L. (2019, July). The Extreme Universe Space Observatory on a Super-
511 Pressure Balloon II Mission. In *36th international cosmic ray conference*
512 (*icrc2019*) (Vol. 36, p. 466).
- 513 Wüst, S., Schmidt, C., Hannawald, P., Bittner, M., Mlynczak, M. G., & Rus-
514 sell III, J. M. (2019). Observations of oh airglow from ground, aircraft,
515 and satellite: investigation of wave-like structures before a minor strato-
516 spheric warming. *Atmospheric Chemistry and Physics*, 19(9), 6401–6418.
517 doi: 10.5194/acp-19-6401-2019
- 518 Zucker, S., & Giryes, R. (2018, mar). Shallow transits—deep learning. i. feasibility
519 study of deep learning to detect periodic transits of exoplanets. *The Astronom-*
520 *ical Journal*, 155(4), 147. doi: 10.3847/1538-3881/aaae05

figure1.eps.

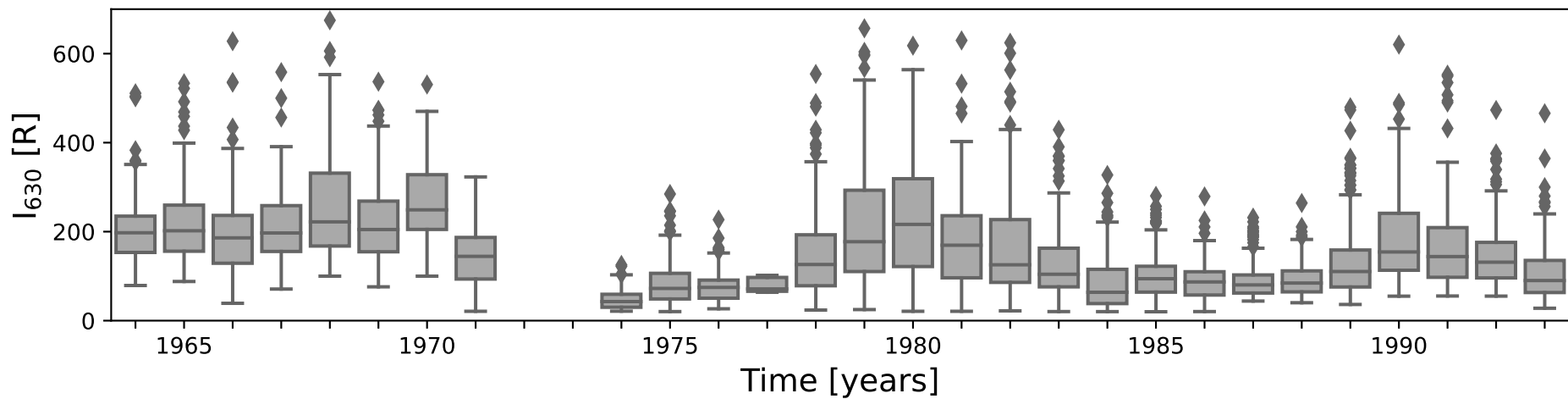
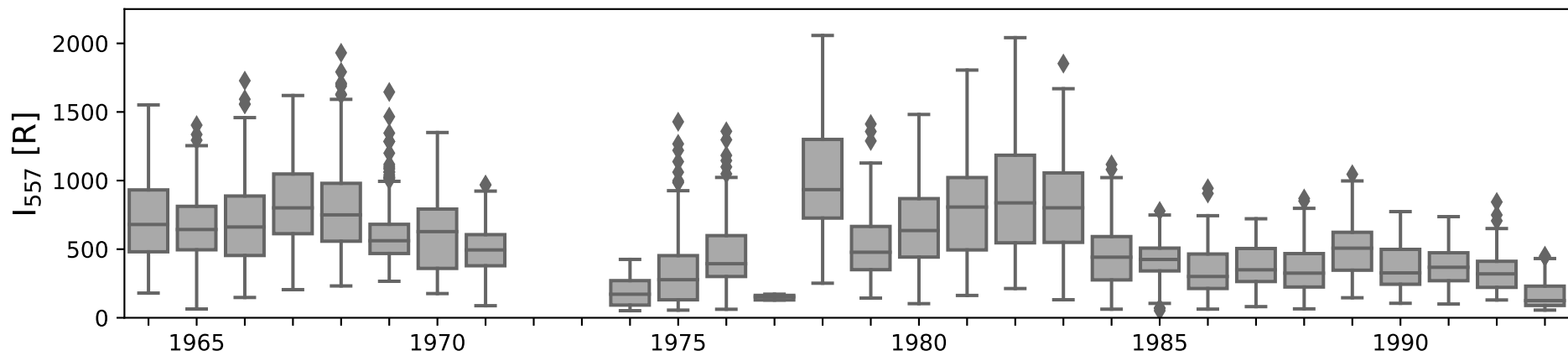


figure2.eps.

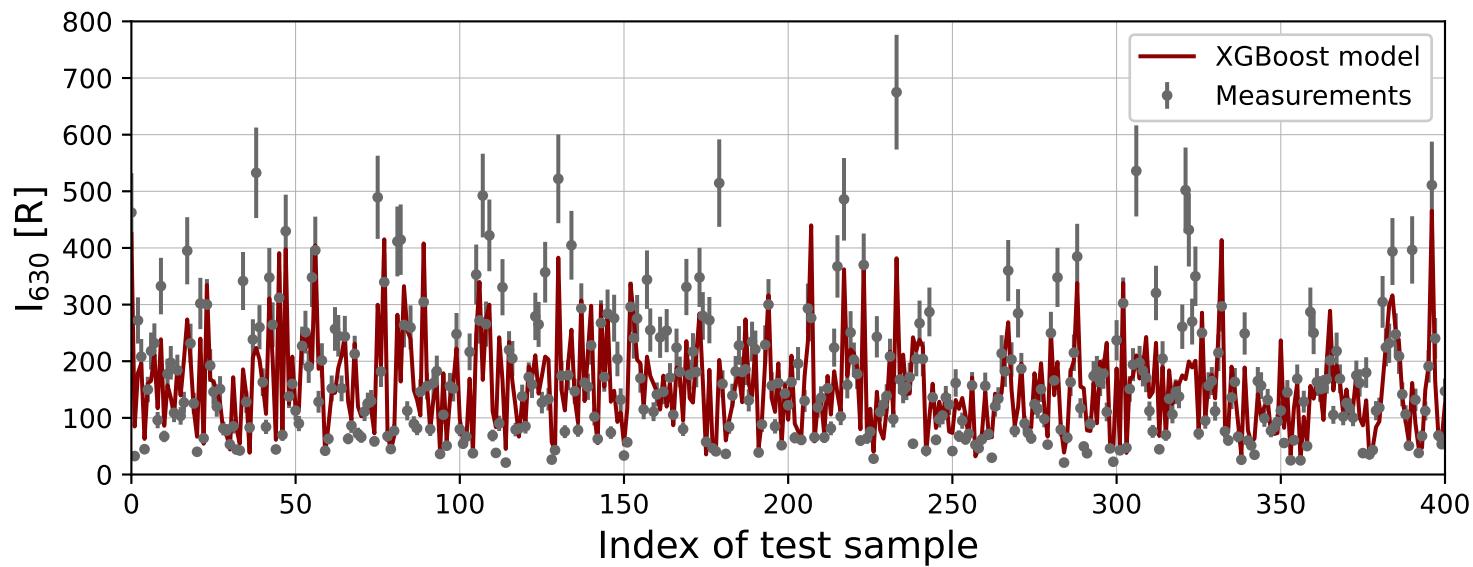
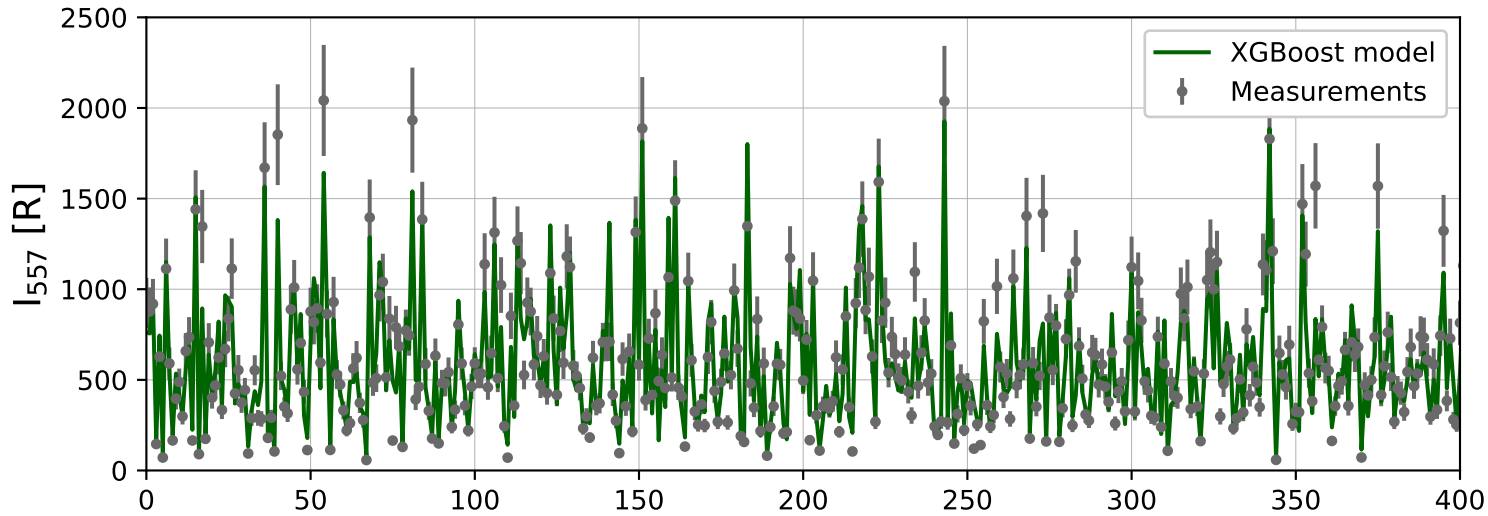


figure3.eps.

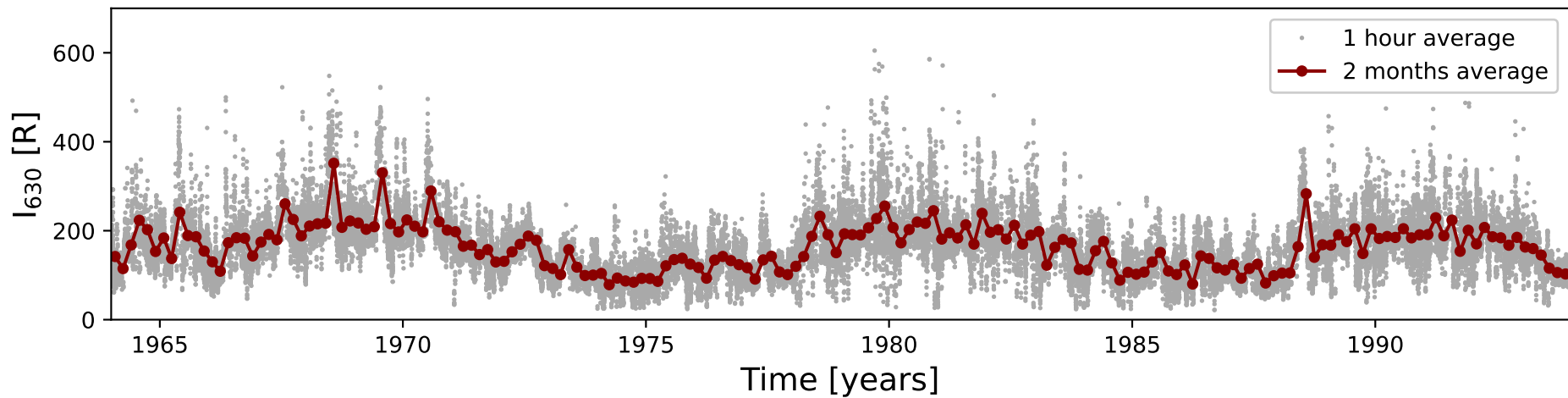
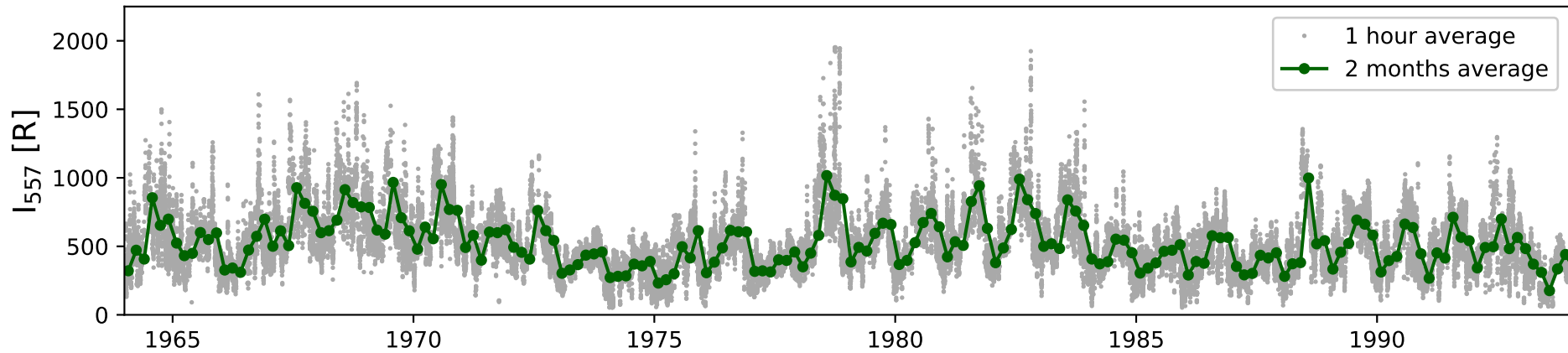


figure4.eps.

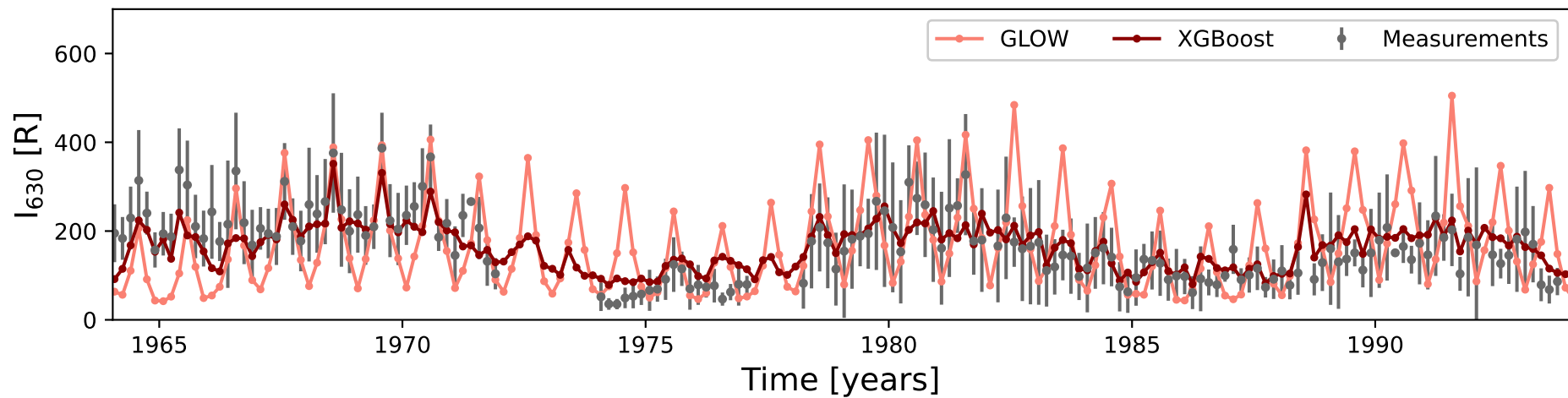
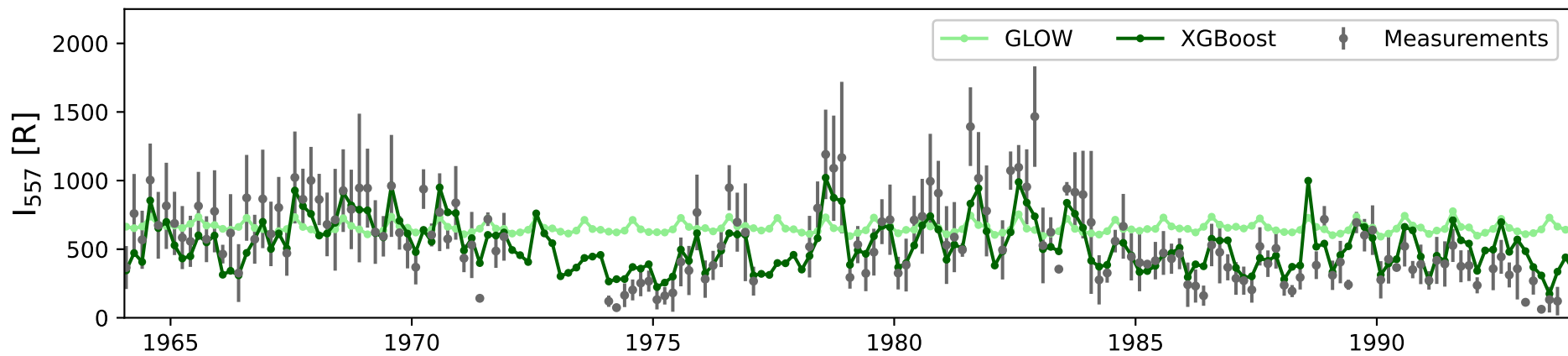


figure5.eps.

